Article

Developmental Cell

miR-263a Regulates ENaC to Maintain Osmotic and Intestinal Stem Cell Homeostasis in *Drosophila*

Graphical Abstract

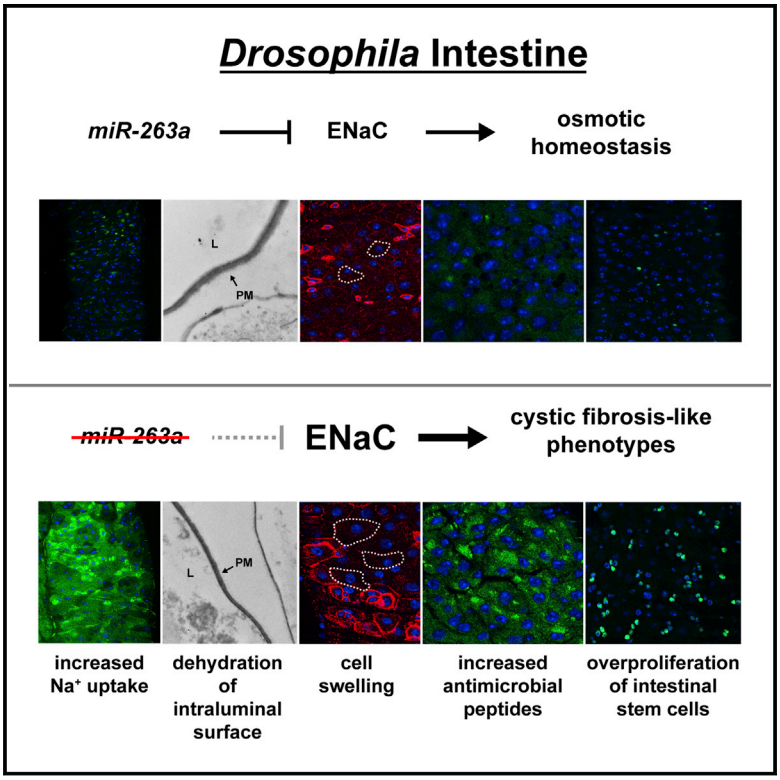

Highlights

- *miR-263a* regulates the expression of ENaC to maintain osmotic and ISC homeostasis
- Loss of *miR-263a* leads to cystic fibrosis-like phenotypes in the *Drosophila* gut
- Overexpression of human *miR-183* can target the expression of human ENaC subunits

Authors

Kevin Kim, Ruei-Jiun Hung, Norbert Perrimon

Correspondence

kkim@genetics.med.harvard.edu (K.K.), perrimon@receptor.med.harvard.edu (N.P.)

In Brief

Kim et al. demonstrate that *miR-263a* regulates the expression of the epithelial sodium channel ENaC to maintain osmotic and intestinal stem cell homeostasis. Furthermore, *miR-263a* mutants display phenotypes that are reminiscent of the pathophysiology of cystic fibrosis, suggesting that *Drosophila* could be used as a model for cystic fibrosis.

Kim et al., 2017, Developmental Cell *40*, 1–14
January 9, 2017
http://dx.doi.org/10.1016/j.devcel.2016.11.023

CellPress

Please cite this article in press as: Kim et al., *miR-263a* Regulates ENaC to Maintain Osmotic and Intestinal Stem Cell Homeostasis in *Drosophila*, Developmental Cell (2016), http://dx.doi.org/10.1016/j.devcel.2016.11.023

Developmental Cell
Article

miR-263a Regulates ENaC to Maintain Osmotic and Intestinal Stem Cell Homeostasis in *Drosophila*

Kevin Kim,[1,3,*] Ruei-Jiun Hung,[1] and Norbert Perrimon[1,2,*]
[1]Department of Genetics
[2]Howard Hughes Medical Institute
Harvard Medical School, Boston, MA 02115, USA
[3]Lead Contact
*Correspondence: kkim@genetics.med.harvard.edu (K.K.), perrimon@receptor.med.harvard.edu (N.P.)
http://dx.doi.org/10.1016/j.devcel.2016.11.023

SUMMARY

Proper regulation of osmotic balance and response to tissue damage is crucial in maintaining intestinal stem cell (ISC) homeostasis. We found that *Drosophila miR-263a* downregulates the expression of epithelial sodium channel (ENaC) subunits in enterocytes (ECs) to maintain osmotic and ISC homeostasis. In the absence of *miR-263a*, the intraluminal surface of the intestine displays dehydration-like phenotypes, Na^+ levels are increased in ECs, stress pathways are activated in ECs, and ISCs overproliferate. Furthermore, *miR-263a* mutants have increased bacterial load and expression of antimicrobial peptides. Strikingly, these phenotypes are reminiscent of the pathophysiology of cystic fibrosis (CF) in which loss-of-function mutations in the chloride channel CF transmembrane conductance regulator can elevate the activity of ENaC, suggesting that *Drosophila* could be used as a model for CF. Finally, we provide evidence that overexpression of *miR-183*, the human ortholog of *miR-263a*, can also directly target the expressions of all three subunits of human ENaC.

INTRODUCTION

The *Drosophila* intestinal system is an attractive model for studying signaling events that control stem cell homeostasis given its anatomical and functional similarities to human epithelial systems, including the intestine (Jiang and Edgar, 2011). The adult midgut is continuously damaged during feeding as well as by chemicals and pathogens they encounter in the food, and thus needs to be constantly renewed. The renewal process requires tight regulation of the activities of multiple conserved signaling pathways in response to various types of intestinal epithelial injuries. These responses promote both intestinal stem cell (ISC) proliferation and enteroblast (EB) differentiation, expediting the rapid generation of new midgut epithelial cells to replace damaged ones (Biteau and Jasper, 2011; Buchon et al., 2010; Jiang and Edgar, 2011; Jiang et al., 2009; Osman et al., 2012; Zhou et al., 2013).

MicroRNAs (miRNAs) are small non-coding RNAs that post-transcriptionally regulate gene expression. In the past few years, miRNAs have been shown to play an important role in stem cell homeostasis by regulating differentiation and self-renewal (Gangaraju and Lin, 2009; Mathieu and Ruohola-Baker, 2013; Yi and Fuchs, 2012). Here, we found that a well-conserved miRNA, *miR-263a*, is necessary for maintaining ISC homeostasis. We show that deletion of *miR-263a* in the adult midgut enterocytes (ECs) activates a stress response that, in turn, activates signaling pathways required for ISC proliferation, resulting in midgut hyperplasia. We identified well-conserved subunits of the epithelial sodium channel (ENaC) as biologically important targets of *miR-263a* and demonstrate that regulation of these subunits by *miR-263a* is critical for maintaining proper osmotic homeostasis in the midgut epithelium. Remarkably, many of the phenotypes of *miR-263a* mutants are reminiscent of the pathophysiology of cystic fibrosis (CF), an autosomal recessive disorder caused by mutations in the gene encoding the chloride channel CF transmembrane conductance regulator (CFTR) (Riordan, 2008). In CF patients, loss-of-function mutations in the CFTR can elevate the activity of ENaC through a mechanism that is not fully understood (Berdiev et al., 2009). ENaC is present at the apical plasma membrane in many epithelial tissues throughout the body to regulate sodium reabsorption, and control total body salt and water homeostasis (Garty and Palmer, 1997). The most common symptoms of CF are potential lethal blockages of distal small intestines, airway mucus obstruction, and chronic airway inflammation (Grubb and Gabriel, 1997; Mall et al., 2004), which are consistent with the model that upregulation in ENaC activity increases sodium and water reabsorption, ultimately leading to dehydration of the intraluminal surface and reduction in mucus transport (Bhalla and Hallows, 2008). Interestingly, we provide evidence that overexpression of *miR-183*, the human ortholog of *miR-263a*, can also directly target all three subunits of human ENaC to regulate its activity. Altogether, our findings describe the role of a miRNA in regulating ENaC levels and suggest that the *Drosophila* intestine could be used as a model for CF.

RESULTS

miR-263a Is Required for ISC Homeostasis

To identify miRNAs that regulate ISC homeostasis, we screened for miRNAs that alter the basal number of ISCs in the adult posterior midgut using publicly available miRNA deletion mutants. From the screen, we identified *miR-263a* as necessary for

Please cite this article in press as: Kim et al., *miR-263a* Regulates ENaC to Maintain Osmotic and Intestinal Stem Cell Homeostasis in *Drosophila*, Developmental Cell (2016), http://dx.doi.org/10.1016/j.devcel.2016.11.023

maintaining ISC homeostasis. Using a homozygous viable null allele of *miR-263a* (*miR-263a*$^{\Delta}$) (Hilgers et al., 2010), we found that *miR-263a* mutants have an increased number of ISCs, as marked by Delta (Dl) expression (Figures 1A and 1B). In addition, many of these ISCs were juxtaposed, suggesting that they undergo symmetric division (Figure 1B). This phenotype is similar to the symmetric division of ISCs seen in *neuralized* and *βν integrin* (*βint-ν*) mutants, where downregulation of Dl/Notch signaling leads to frequent ISC duplication, expanding the pool of ISCs (Ohlstein and Spradling, 2007; Okumura et al., 2014).

To determine where in the midgut epithelium *miR-263a* is expressed, we took advantage of a *Gal4* knockin allele of *miR-263a* (*miR-263a*$^{\Delta}$*-Gal4*), in which the *miR-263a* hairpin sequences are replaced by *Gal4* (Hilgers et al., 2010) to drive the expression of a *UAS-GFP* transgene, thus marking all cells that express *miR-263a*. GFP expression was restricted to ECs, as evidenced by a lack of GFP expression in either ISCs or EBs, which were marked with *esg-LacZ* (Figures S1A–S1A″), or in enteroendocrine cells, which were marked with immunostaining of Prospero (Pros) (Figures S1B–S1B″).

To discover whether the increased number of ISCs was due to an increase in proliferation, we stained the midguts using anti-phospho-histone H3 (pH3), a marker for cells undergoing mitosis (Figures 1C and 1D). In *miR-263a* mutants, the average number of pH3^{+} cells increased with age while the numbers of pH3^{+} cells were relatively constant in the control (Figures 1E and S1C). Although *miR-263a* mutants had higher averages of pH3^{+} cells in both 7- and 14-day-old guts compared with controls, only the 14-day-old average was statistically different. Overexpression of a *miR-263a* in a *miR-263a* mutant background completely suppressed the increase in pH3^{+} cells (Figure 1E), indicating that the phenotype was due to the absence of functional *miR-263a*.

Next, we assessed the impact of *miR-263a* on overall midgut proliferation by generating *miR-263a* mutant clones using the MARCM (mosaic analysis with a repressible cell marker) approach (Lee and Luo, 2001). Clones of *miR-263a* mutant cells grew larger than control clones (Figures 1F–1I, S1D, and S1E), consistent with an increase in ISC proliferation. Furthermore, *miR-263a* mutant clones induced non-cell-autonomous ISC proliferation, as indicated by an increased number of pH3^{+} and Dl^{+} cells outside the mutant clones (Figures 1F–1I″). These results indicate that loss of *miR-263a* expression in the ECs can have a non-cell-autonomous effect on ISC homeostasis.

Surprisingly, the *miR-263a* mutation also had an effect on the overall morphology of the adult midgut. The posterior midguts of the *miR-263a* mutants were shorter in length and larger in width compared with controls (Figures S1F–S1K). We further observed that shortening and thickening of the midgut was due to multi-layering of the epithelium (Figures S1L–S1N). In addition, we observed that multi-layering of epithelial cells was followed by delamination and anoikis of ECs, which is evident by the presence of large lysosomes (Figure S1O).

Absence of *miR-263a* Induces Stress and Developmental Signaling Pathways to Promote ISC Hyperproliferation

In the midgut the Jun N-terminal kinase (JNK) pathway is activated in response to EC stress/damage to promote ISC proliferation and differentiation, leading to rapid regeneration of the epithelium to replace damaged ECs (Jiang et al., 2009). To test whether ECs in *miR-263a* mutants are stressed/damaged, we used a *puckered* (*puc*) *LacZ* reporter line (*puc-LacZ*) to monitor JNK pathway activity. Using the MARCM approach, we generated *miR-263a* mutant clones and observed high levels of JNK pathway activation in both mutant clones and neighboring cells (Figures 2A and 2B″). This non-cell-autonomous activation of the JNK pathway is likely caused by ECs that are detaching from the basement membrane due to their larger and more proliferative neighboring *miR-263a* mutant clones. In a recent study, *Notch*-defective ISC tumors have been shown to displace surrounding ECs, competing with them for basement membrane space and causing their detachment, extrusion, and apoptosis (Patel et al., 2015). In fact, the multi-layering phenotypes of the *miR-263a* mutant midgut (Figures S1M and S1N) are very similar to the EC detachment phenotype observed in the previous study. Furthermore, this non-cell-autonomous activation of the JNK pathway likely stimulates the proliferation of neighboring ISCs (Figures 1I–1I″), which may further expand the expression of *puc-LacZ*.

Upon activation of the JNK pathway, damaged ECs and surrounding visceral muscle (VM) release ligands that activate JAK/STAT and EGFR/Ras/MAPK signaling pathways to promote ISC proliferation and differentiation (Biteau and Jasper, 2011; Buchon et al., 2010; Jiang and Edgar, 2011; Jiang et al., 2009; Osman et al., 2012; Zhou et al., 2013). Therefore, we examined the expression of these ligands in *miR-263a* mutant midguts using real-time qPCR. Indeed, we found that expression of the *Unpaired* cytokines (*Upd*, *Upd2*, and *Upd3*), which activate JAK/STAT signaling, and EGFR ligands, *vein* (*vn*), *Spitz* (*Spi*), and *Keren* (*Krn*), were significantly induced (Figure S2). Next, we examined whether induction of these ligands truly activates JAK/STAT and EGFR/Ras/MAPK signaling. To measure JAK/STAT pathway activity, we used a *Stat92E* reporter line driving the expression of GFP (*10xSTAT-GFP*). In control, the expression of *10xSTAT-GFP* was restricted to ISCs and EBs (Figure 2C), while large patches of cells expressed the reporter in the *miR-263a* mutant (Figure 2D). Furthermore, the expression of *10xSTAT-GFP* was also present in large misdifferentiated EC-like polyploid cells. To monitor EGFR/Ras/MAPK pathway activity, we examined the levels of phosphorylated ERK (dpERK) (Gabay et al., 1997). In control, dpERK signals were weakly detected in ISCs and EBs (Figures 2E and 2E′). However, in *miR-263a* mutants, ectopic dpERK signals were mainly observed in large differentiated ECs (Figures 2F and 2F′). Collectively, these results demonstrate that loss of *miR-263a* in the midgut activates the JNK pathway, which in turn increases the production of both JAK/STAT and EGFR/Ras/MAPK pathway ligands to promote hyperproliferation of ISCs.

Identification of Putative *miR-263a* Targets

To further understand the molecular function of *miR-263a* in maintaining ISC homeostasis, we searched for *miR-263a* target genes using TargetScan (Ruby et al., 2007), which predicted 158 targets. Since *miR-263a* expression is specific to ECs in the adult midgut, we cross-referenced the list of predicted *miR-263a* target genes with a list of genes that we identified to be specifically expressed in ECs, using the cell-type-specific gene expression profiling technique TADA (Southall et al., 2013) (targeted DNA adenine methyltransferase identification using the

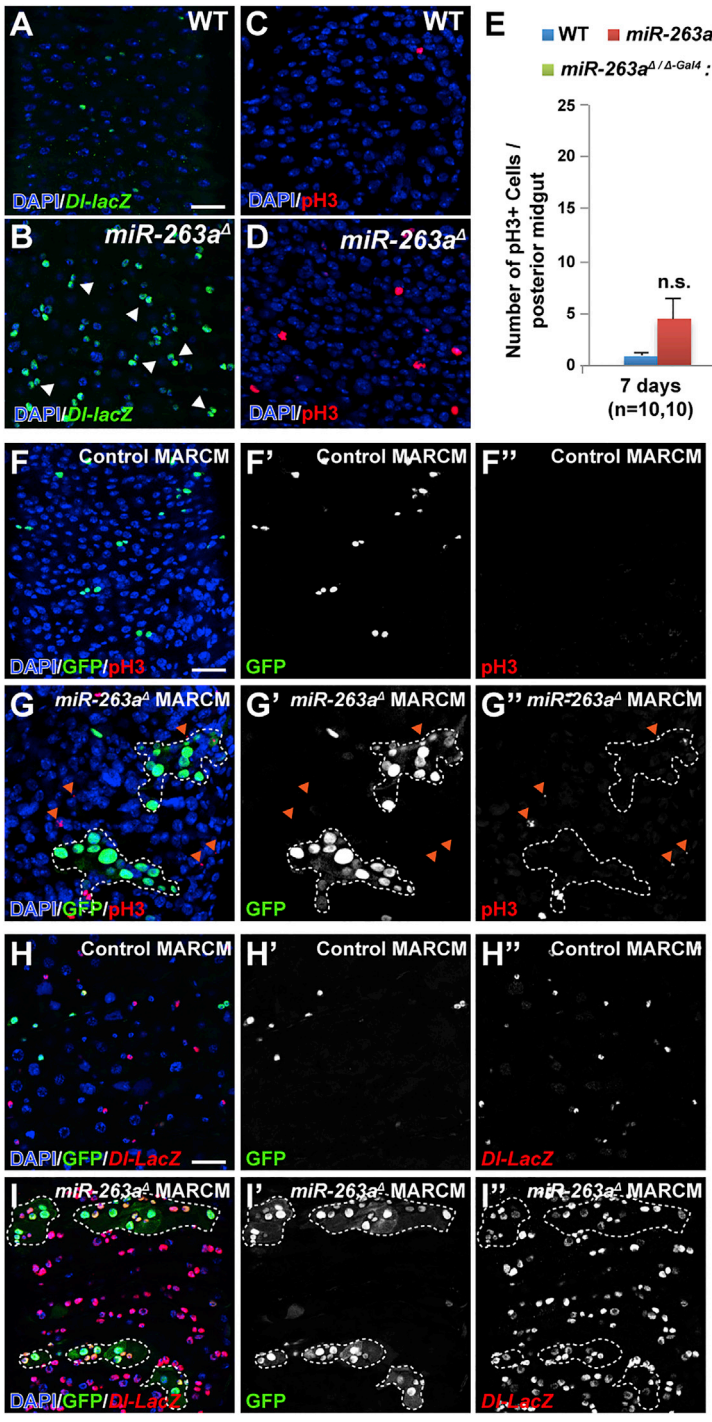

Figure 1. Phenotypes of *miR-263a* Mutant

(A and B) The posterior midguts of 14-day-old wild-type (WT) and *miR-263a* mutant stained with anti-β-gal to mark Dl (green). White arrowheads mark symmetrically divided ISCs (B). The scale bar represents 25 μm.

(C and D) The posterior midguts of wild-type and *miR-263a* mutant stained with anti-pH3 to mark mitotic ISCs (red).

(E) The average number of pH3$^+$ cells in the posterior midguts at 7 and 14 days old. n denotes the number of posterior midguts examined for each genotype. Error bars indicate SEM. ***$p < 0.001$ (two-tailed t test).

(F–I″) MARCM clones are labeled with GFP. White dotted lines outline the *miR-263a* mutant clones. (F–G″) *miR-263a* mutant clones can induce ISC proliferation non-cell-autonomously as indicated by the increased number of pH3$^+$ cells (red) outside the mutant clones (orange arrowheads). (H–I″) Non-cell-autonomous increase in the number of ISCs, marked with *Dl-LacZ* (red), was observed outside the *miR-263a* mutant clones. The scale bar represents 25 μm.

See also Figure S1.

RNA polymerase II-DAM fusion protein; D. Doupé and N. Perrimon, personal communication), thus restricting the list to 32 genes. Next, we examined the transcript levels of all 32 genes by qPCR and found that five genes had elevated transcript levels (>2-fold on average) in the *miR-263a* mutant midguts compared with the control (Table S1). Interestingly, one gene, *Nach*, had approximately 41-fold higher transcript level in the mutant compared with the control (Table S1 and Figure 3A). Furthermore, we raised an antibody against Nach and found that mutant midguts had significantly more Nach proteins, whereas it was undetectable in the control (Figures 3B and 3C). These striking increases in both the transcript and protein levels prompted us to further investigate whether *Nach* is a functionally important target of *miR-263a* in the adult midgut.

Nach Is a Functional Target of *miR-263a* in the Adult Posterior Midgut Epithelium

In *Drosophila*, *Nach* (also known as *ppk4*) is one of 31 family members (termed *pickpocket* [*ppk*] genes) that represent ion channels called the Degenerin/epithelial sodium channel (DEG/ENaC) (Zelle et al., 2013). Although the physiological functions of most family members are not known, some have been shown to act as non-voltage-gated sodium channels (Bianchi and Driscoll, 2002; Garty and Palmer, 1997). The *Nach* 3′ UTR contains three potential *miR-263a* binding sites (Figure S3A). To determine whether *miR-263a* regulates the expression of *Nach* through these binding sites, we generated a luciferase reporter carrying the full-length *Nach* 3′ UTR. Co-expression of the *Nach* 3′ UTR luciferase reporter with *miR-263a* in *Drosophila* S2R$^+$ cells significantly reduced luciferase activity, while mutating the *miR-263a* seed sequences, the minimal sequence required for silencing of targets (Brennecke et al., 2005), completely relieved the suppression (Figure 3D). These results suggest that *miR-263a* can directly regulate the expression of *Nach* through these binding sites.

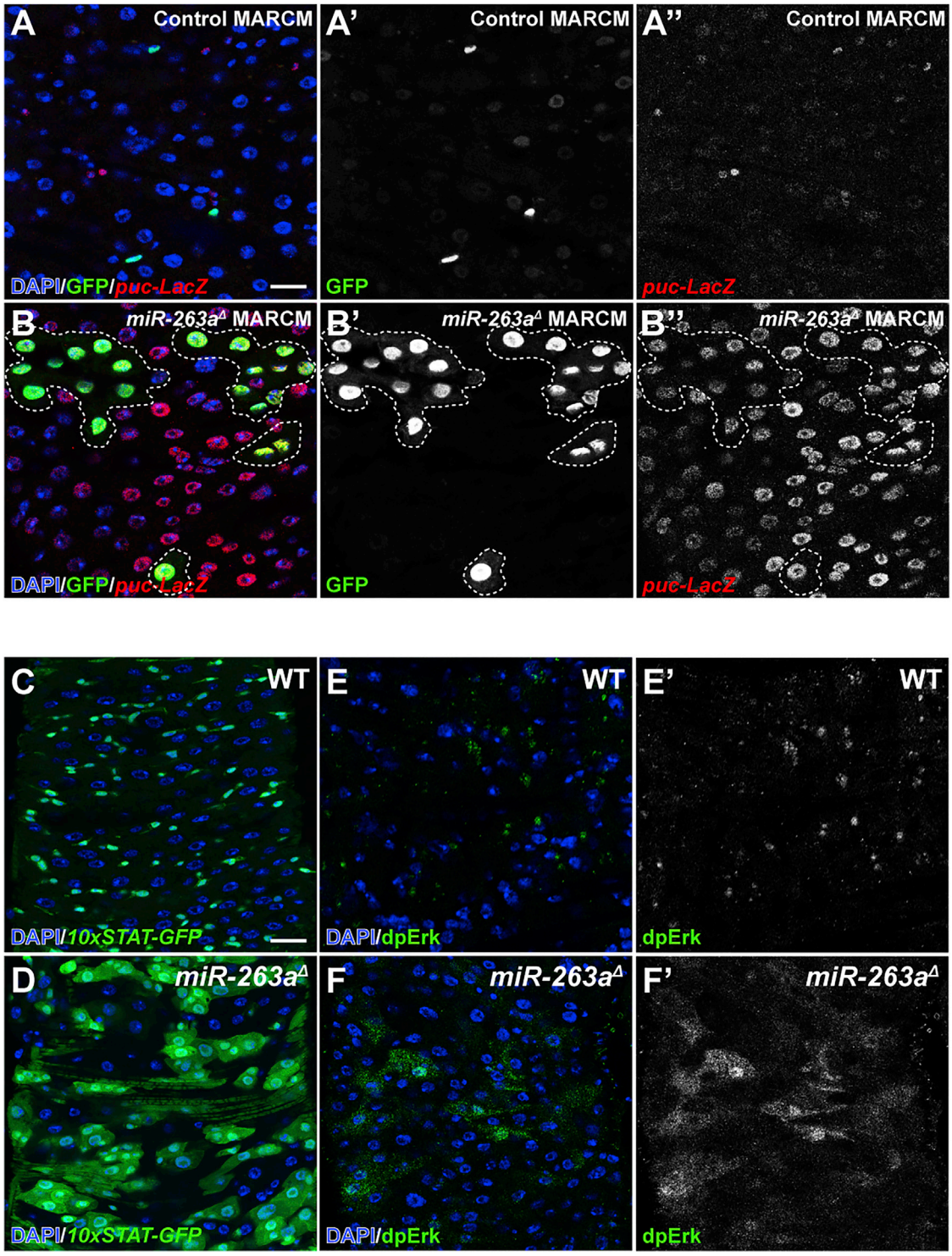

Figure 2. Absence of *miR-263a* Activates Stress and Developmental Signaling Pathways

(A–B″) Activation of the JNK pathway in *miR-263a* mutants as visualized by the increased number of *puc-LacZ*-expressing cells. White dotted lines outline *miR-263a* mutant clones.

(C and D) Enhancement of JAK/STAT pathway activity in *miR-263a* mutants as visualized by the increased expression of *10xSTAT-GFP* reporter.

(E–F′) Enhancement of EGFR pathway activity in *miR-263a* mutants as visualized by the increased expression of dpERK.

The scale bars represents 25 μm. See also Figure S2.

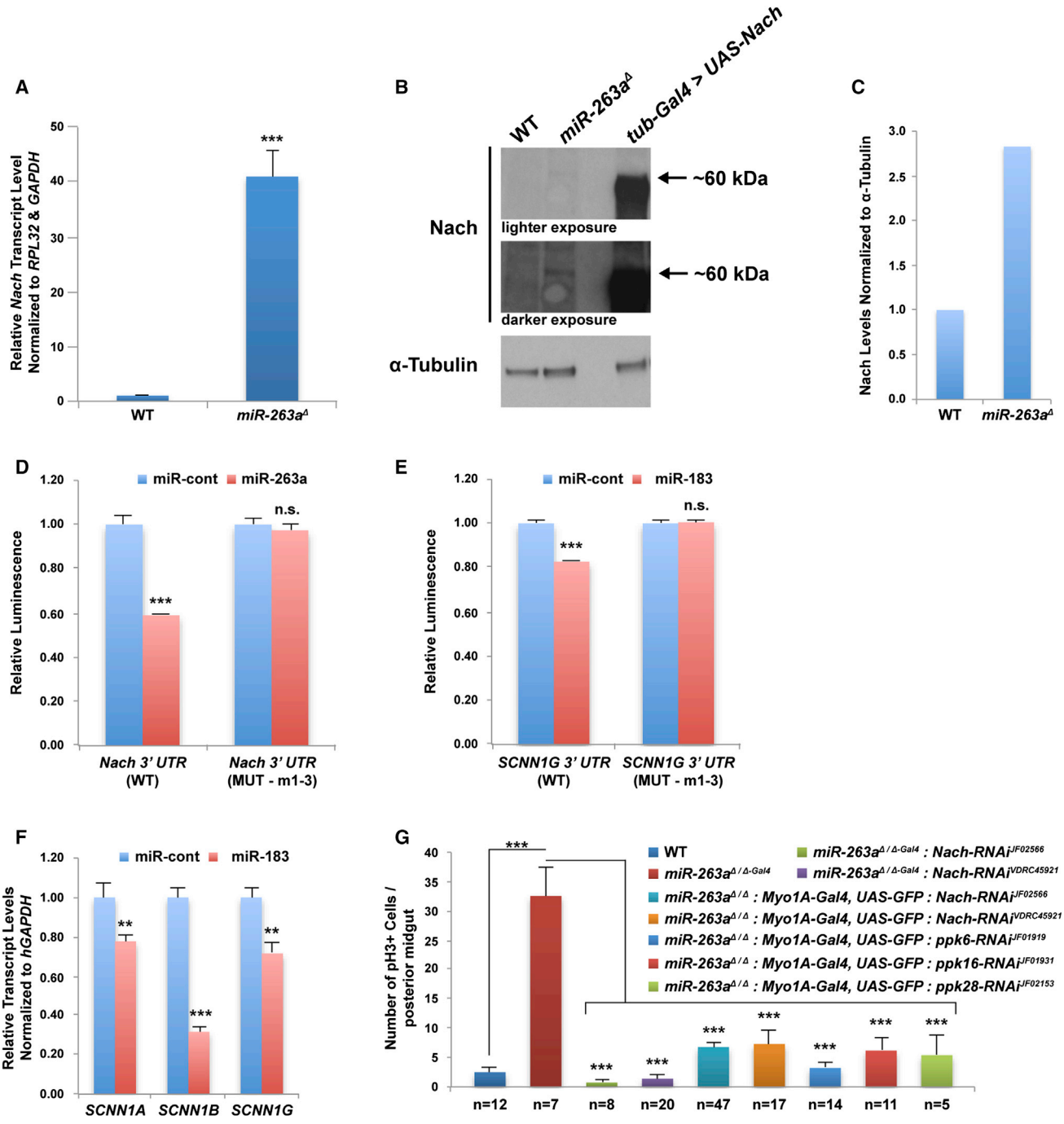

Figure 3. Regulation of ENaC by *miR-263a*

(A) Relative *Nach* transcript level in *miR-263a* mutant midguts.

(B) Western blot analysis of Nach in *miR-263a* mutant midguts. α-Tubulin was used as loading control.

(C) Quantitative analysis of the western blot from (B).

(D) *Nach* 3′ UTR luciferase reporter assay.

(E) *SCNN1G* 3′ UTR luciferase reporter assay.

(F) Relative transcript levels of human ENaC subunits after overexpression of *miR-183* in CFBE41o$^-$ cells.

(G) The average number of pH3$^+$ cells in the posterior midguts at 14 days old. Depletion of *Nach* using two independent RNAi lines and two different *Gal4* drivers in the *miR-263a* mutant background suppressed the increased number of pH3$^+$ cells. The phenotype was also suppressed when other ENaC subunits were depleted in the mutant background.

n denotes the number of posterior midguts examined for each genotype. Error bars indicate SEM. **$p < 0.05$ and ***$p < 0.001$ (two-tailed t test). See also Figure S3 and Table S1.

Drosophila encodes a second miRNA closely related in sequence to *miR-263a* called *miR-263b*. Interestingly, homozygous null mutants of *miR-263b* do not perturb ISC homeostasis (Figure S1C). One possibility is that slight differences in *miR-263a* and *miR-263b* seed sequences allow each miRNA to target a different set of genes. In fact, *Nach* is not a predicted target of *miR-263b*. Nevertheless, both *miR-263a* and *miR-263b* are members of a conserved family of miRNAs that includes mammalian *miR-183*, *miR-96*, and *miR-182*. The high degree of sequence conservation prompted us to ask whether human *miR-183*, the miRNA most closely related in sequence to *miR-263a*, has analogous function in regulating the activity of ENaC. In humans, three genes termed *sodium channel*, *non-voltage-gated 1* (*SCNN1*) *alpha*, *beta*, *and gamma* (*SCNN1A*, *SCNN1B*, and *SCNN1G*, respectively) encode components of the heteromultimeric ENaC (Canessa et al., 1994; Lingueglia et al., 1993; Waldmann et al., 1995). Based on ortholog prediction (Hu et al., 2011), *Nach* has two predicted orthologs, *SCNN1G* and *SCNN1B*; however, *Nach* is more closely related to *SCNN1G*. Strikingly, *SCNN1G* 3′ UTR contains three potential *miR-183* binding sites (Figure S3B), and co-expression of the *SCNN1G* 3′ UTR luciferase reporter with *miR-183* modestly but significantly reduced luciferase activity, whereas mutating the *miR-183* seed regions completely relieved the suppression (Figure 3E).

To further investigate the inhibitory potential of *miR-183* on *SCNN1G*, we performed qPCR analyses to measure the endogenous transcript level of *SCNN1G* after overexpressing *miR-183*. We used immortalized human CF bronchial epithelial (CFBE41o$^-$) cells, bearing the most frequent mutation in the CFTR gene (ΔF508), which has increased ENaC activity. Overexpression of *miR-183* in CFBE41o$^-$ cells significantly reduced the endogenous *SCNN1G* transcript level (Figure 3F), likely through the three *miR-183* binding sites we identified (Figure S3B). Strikingly, we also observed significant decreases in the endogenous transcript levels of *SCNN1A* and *SCNN1B* (Figure 3F). To investigate whether these are also due to direct interactions with *miR-183*, we searched for *miR-183* binding sites and found multiple sites (Figures S3C and S3D). Co-expression of the 3′ UTR luciferase reporters with *miR-183* also modestly but significantly reduced the luciferase activities (Figure S3F). These results demonstrate that overexpression of *miR-183* can repress ENaC activity by directly targeting all three ENaC subunits.

To investigate whether misregulation of *Nach* contributes to the overproliferation of ISCs in *miR-263a* mutants, we depleted *Nach* in the *miR-263a* mutant background. Depletion of *Nach* by RNAi suppressed the increase in pH3$^+$ cells (Figure 3G). In addition, to address whether Nach activity was required for proliferation of ISCs in general, we examined the consequence of depleting Nach activity on proliferation of ISCs in a gut regeneration model induced by feeding flies with dextran sodium sulfate (DSS) or bleomycin (Jiang et al., 2009; Ren et al., 2010). Knockdown of *Nach* did not suppress DSS or bleomycin-induced proliferation of ISCs (Figure S3H), indicating that *Nach* is dispensable for damage-induced ISC proliferation.

In mammals, overexpression of either *SCNN1A* or *SCNN1B* subunit alone is sufficient for ENaC activity (Canessa et al., 1994; Mall et al., 2004). Therefore, we asked whether overexpression of Nach alone is sufficient to disrupt ISC homeostasis by increasing ENaC activity. Overexpression of Nach in an otherwise wild-type background failed to increase the number of pH3$^+$ cells (Figure S3I), suggesting that Nach may require additional subunits for full ENaC activity. This result led us to hypothesize that additional ENaC subunits may be misregulated in the *miR-263a* mutant, and therefore began searching for other ENaC subunits in flies. Out of 12 *ppk* genes that are predicted orthologs of human *SCNN1* genes, only four *ppk* genes (*Nach*/*ppk4*, *ppk6*, *ppk16*, and *ppk28*) are expressed in ECs (Figure S3J) (D. Doupé and N. Perrimon, personal communication), and all have elevated expression in *miR-263a* mutant midguts (Figures 3A and S3K). Depleting individual *ppk* genes by RNAi in the *miR-263a* mutant background suppressed the increase in pH3$^+$ cells (Figure 3G), suggesting that together with Nach they may form a functional ENaC in flies. To determine whether this regulation is direct, we searched and found potential *miR-263a* binding sites in all three putative fly ENaC subunits (*ppk6*, *ppk16*, and *ppk28*) and performed 3′ UTR luciferase assays. We found that *miR-263a* was, in addition to *Nach*, only able to directly regulate the expression of *ppk28* (Figures S3E and S3G). Collectively, these results suggest that *miR-263a* can directly and indirectly regulate the expressions of multiple candidate ENaC subunits.

Sodium Levels Increase in *miR-263a* Mutant Midgut Epithelium

To examine whether misregulation of ENaC subunits in *miR-263a* mutants leads to Na^+ imbalance in the midgut epithelium, we used an Na^+-sensitive fluorescent indicator, Sodium Green, to observe the amount of Na^+ in the midgut epithelium. Sodium Green is frequently used to provide spatial and temporal resolution of Na^+ concentrations with sufficient selectivity in the presence of physiological concentrations of other monovalent cations (Amorino and Fox, 1995; Minta and Tsien, 1989). Overall, *miR-263a* mutants displayed a higher amount of intracellular Na^+ along the entire length of the midgut as indicated by the increased fluorescence, with three very distinct regions where the increase was most significant (Figures S4A and S4B). Since many of the *miR-263a* mutant phenotypes we observed are manifested in the posterior region of the midgut, we focused our analyses on this specific region. The posterior midguts of *miR-263a* mutants had an approximately 4- to 5-fold higher amount of intracellular Na^+ compared with control (Figures 4A, 4B′, S4C, S4C′, and S4H), suggesting that they are allowing more Na^+ across the epithelial membrane. Although disruption of the cell membrane in ECs undergoing delamination and anoikis may allow uptake of more Sodium Green and increase the fluorescent signal in the *miR-263a* mutants, only a small percentage of the ECs undergo delamination and anoikis; therefore, we do not believe that dying cells are the major contributors of increased Sodium Green fluorescence. Overexpression of *miR-263a* or depletion of *Nach* and other ENaC subunits in the *miR-263a* mutant background completely suppressed the phenotype (Figures 4C–4D′, S4D–S4G′, and S4H). Interestingly, while overexpression of Nach alone failed to increase the number of pH3$^+$ cells, we observed an increase in the amount of Na^+ uptake in the midgut epithelium (Figures 4E and 4E′). Quantification of Sodium Green fluorescence revealed an approximately 2-fold increase in the intracellular Na^+ levels, which is modest compared with the intracellular Na^+ of the *miR-263a* mutants (Figure S4H). This result suggests that

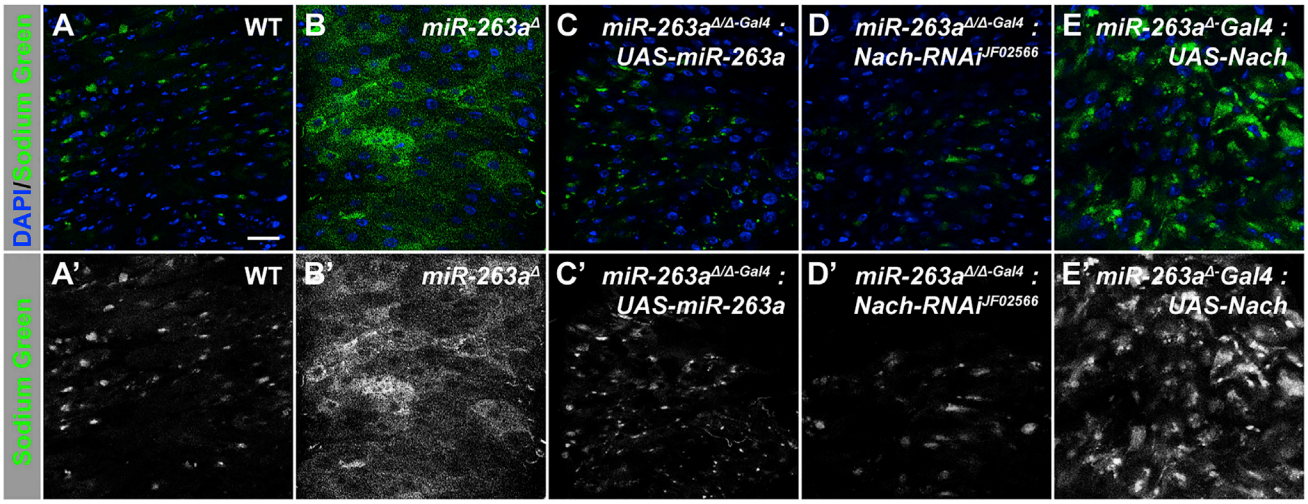

Figure 4. Increased Na^+ in the *miR-263a* Mutant Posterior Midgut Epithelium

(A and A′) Na^+ in the midgut epithelium of control midgut.

(B and B′) Enhancement of Na^+ in the *miR-263a* mutant midgut epithelium.

(C–D′) Suppression of increased Na^+ uptake by overexpressing *miR-263a* (C and C′) or depleting *Nach* (D and D′) in the mutant background.

(E and E′) Overexpression of Nach partially increased the amount of Na^+ in the midgut epithelium.

The scale bar represents 25 μm. See also Figure S4.

overexpression of Nach may partially increase ENaC activity, but not enough to stimulate ISC overproliferation. Collectively, these results suggest that increased intracellular Na^+ in the *miR-263a* mutant midgut epithelium is due to upregulation of ENaC activity as a result of misregulation of multiple ENaC subunits.

Reduced PM Thickness and EC Swelling Phenotypes in the *miR-263a* Mutant Midgut Epithelium

As an increase in ENaC activity can increase sodium and water reabsorption, ultimately leading to dehydration of the intraluminal surface and reduction in mucus transport (Bhalla and Hallows, 2008), we examined the midgut lumen and the features of the peritrophic matrix (PM), which plays a role analogous to that of mucous secretions in the vertebrate digestive tract, for signs of dehydration. Electron microscopy of posterior midgut sections revealed that the thickness of the PM in *miR-263a* mutants was significantly reduced (Figures 5A, 5B, and 5E), and the phenotype was completely suppressed by either depleting *Nach* or overexpressing *miR-263a* in the mutant background (Figures 5C–5E). Interestingly, either overexpression of *miR-263a* or depletion of *Nach* in the mutant background resulted in thicker PM compared with the control (Figure 5E). Thus, reducing *Nach* levels by both *miR-263a* overexpression and *Nach* RNAi may further reduce sodium and water reabsorption, possibly hyperhydrating the PM and causing it to be thicker.

To investigate whether reduction in PM production was responsible for the reduced PM thickness in *miR-263a* mutants, we measured the transcript levels of *drosocrystallin* (*dcy*), an integral component of the PM (Kuraishi et al., 2011). Strikingly, *dcy* levels were approximately 16.5-fold higher in the *miR-263a* mutant midguts compared with the control (Figure S5A). In CF lung disease, excess mucus production and increased transcript levels of *MUC5AC* and *MUC5B*, major secreted gel-forming mucins in human airways (Davies et al., 1999; Hovenberg et al., 1996), are common (Hauber et al., 2004; Henderson et al., 2014), which results in mucus with concentrated mucins that collapses onto the underlying epithelium as a first step toward chronic infection and organ disease (Boucher, 2007; Chen et al., 2010; Matsui et al., 1998). Similarly, we found that transcripts of *Hemolectin* (*Hml*), a close ortholog of both the human *MUC5AC* and *MUC5B* (Hu et al., 2011), are significantly higher in the *miR-263a* mutant midguts (Figure S5B). Collectively these results suggest that, similar to the CF airway, misregulation of ENaC in the *miR-263a* mutant midguts results in increased PM production, and that reduced PM thickness is not due to reduced PM production.

In *Caenorhabditis elegans*, gain-of-function mutations in the orthologs of ENaC (*mec-4*, *mec-10*, and *deg-1*) have been demonstrated to cause vacuolation, cell swelling, and eventual cell lysis (Chalfie and Sulston, 1981; Chalfie and Wolinsky, 1990; Driscoll and Chalfie, 1991; Huang and Chalfie, 1994). Interestingly, we also frequently observed larger ECs in *miR-263a* mutant midguts, suggesting that they may also be swollen. Staining of the midgut cell membrane, using antibodies against Armadillo (Arm), revealed that *miR-263a* mutant ECs have a larger surface area compared with wild-type ECs (Figures 5F–5H). In addition, 3D reconstruction of 2D serial sections of ECs revealed that *miR-263a* mutant ECs have nearly twice the cell volume compared with control ECs (Figure 5I). Next, although we saw a clear increase in the *dcy* and *Hml* transcript levels in *miR-263a* mutant midguts, we further investigated whether genetically disrupting the PM production/thickness was also sufficient to cause EC swelling and hyperproliferation of ISCs. Using a previously characterized loss-of-function allele of *dcy* (*dcy*^{1}) (Kuraishi et al., 2011), we found that *dcy* mutant ECs were comparable in size with the control ECs, and that *dcy* mutants did not disrupt ISC homeostasis (data not shown). Collectively these results suggest that EC swelling is not a direct consequence of reduced PM production/thickness but, rather, that increased

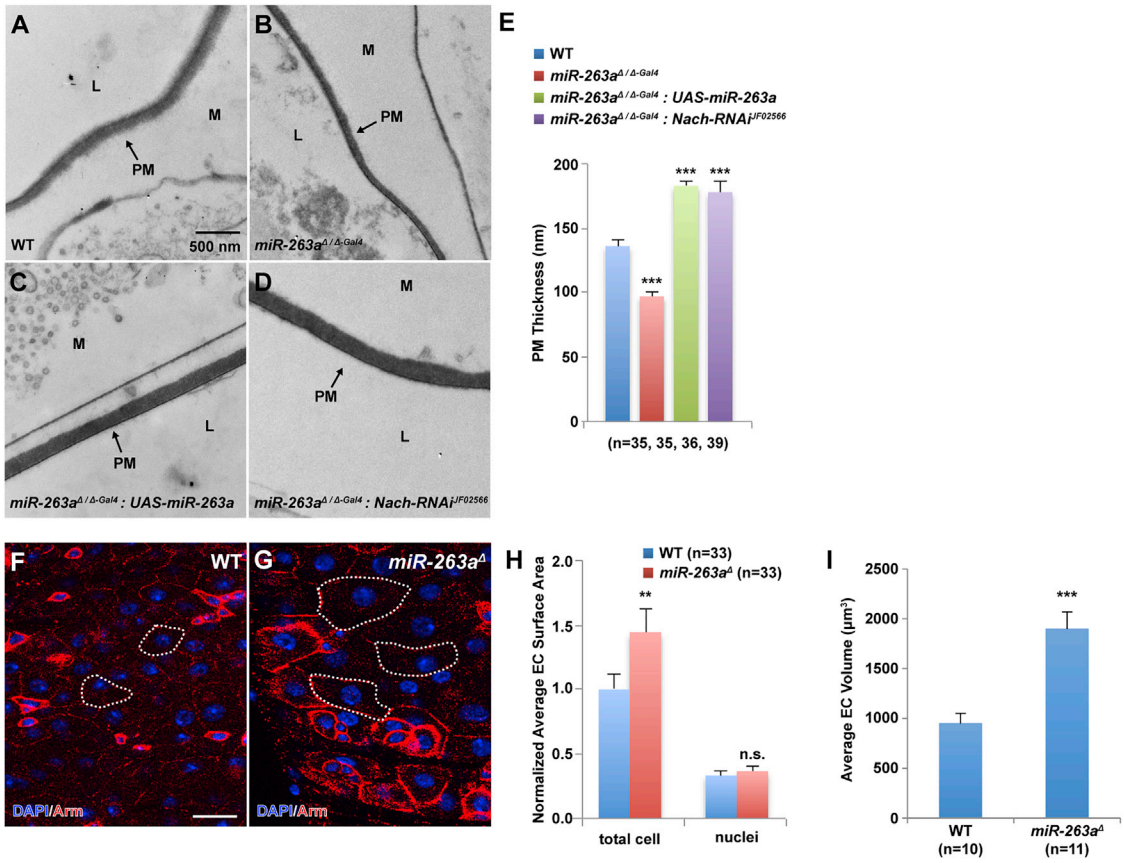

Figure 5. Increased ENaC Activity Disrupts Intestinal Homeostasis in *miR-263a* Mutants

(A–D) EM cross-sections of posterior midguts. *miR-263a* mutants (B) show reduced PM thickness compared with wild-type (WT) (A). Overexpression of *miR-263a* (C) and depletion of *Nach* (D) in the mutant background. Arrows indicate the peritrophic matrix (PM), mucus (M), and lumen with digested food (L).

(E) Quantitative measurements of the PM thickness. n denotes the number of PM thickness measurements for each genotype.

(F and G) Enlarged ECs in the *miR-263a* mutants visualized by anti-Arm marking the cell membrane. White dotted lines outline the representative ECs. The scale bar represents 10 μm.

(H) Normalized quantitative measurements of the total EC and their respective nuclei surface area. n denotes the number of surface area measurements for each genotype.

(I) Quantitative measurements of the total EC volume. n denotes the number of cell-volume measurements for each genotype. Error bars indicate SEM.

$^{**}p < 0.05$ and $^{***}p < 0.001$ (two-tailed t test). See also Figure S5.

expressions of ENaC subunits in the *miR-263a* mutant midgut epithelium leads to swelling of ECs through increased sodium and water reabsorption.

Increased Bacterial Load in *miR-263a*

Because structurally compromising the PM is also associated with increased susceptibility to bacterial infections (Kuraishi et al., 2011), we asked whether *miR-263a* mutants are more susceptible to bacterial infection. Since studies have shown that the Imd pathway regulates antimicrobial peptide production in the gut and plays an important function in the resistance against bacterial infections (Liehl et al., 2006; Nehme et al., 2007; Ryu et al., 2006), we examined the activity of the Imd pathway by measuring the expression of the antimicrobial peptide genes *Attacin A* (*AttA*) and *Diptericin* (*Dpt*), and the nuclear factor κB-like transcription factor *Relish* (*Rel*) in mutant midguts. qPCR analyses revealed that *miR-263a* mutants showed a stronger induction of all three genes (Figure 6A). Next, to directly visualize antimicrobial peptide expression in the midgut, we used a *Drosomycin* (*Drs*) reporter line driving the expression of GFP (*Drs-GFP*). As expected, *miR-263a* mutants expressed a higher level of *Drs-GFP* compared with controls (Figures 6B–6C′).

To determine whether increased activation of the Imd pathway is a direct result of increased bacterial accumulation in the *miR-263a* mutant midgut, we quantified internal bacterial loads by measuring colony-forming units (CFUs). Strikingly, the internal bacterial load in *miR-263a* mutants was significantly higher compared with the controls (Figure 6D). The observed increase in bacterial load in *miR-263a* mutants prompted us to investigate whether an inflammatory response to bacteria accumulation was causing ISC overproliferation. To test this hypothesis, we cultured control and *miR-263a* mutant flies in food containing antibiotics, which eliminated all internal bacteria (Figure 6E). Treatment with antibiotics did not suppress ISC overproliferation in the *miR-263a* mutants (Figure 6E), indicating that bacterial accumulation is not the primary cause of ISC proliferation.

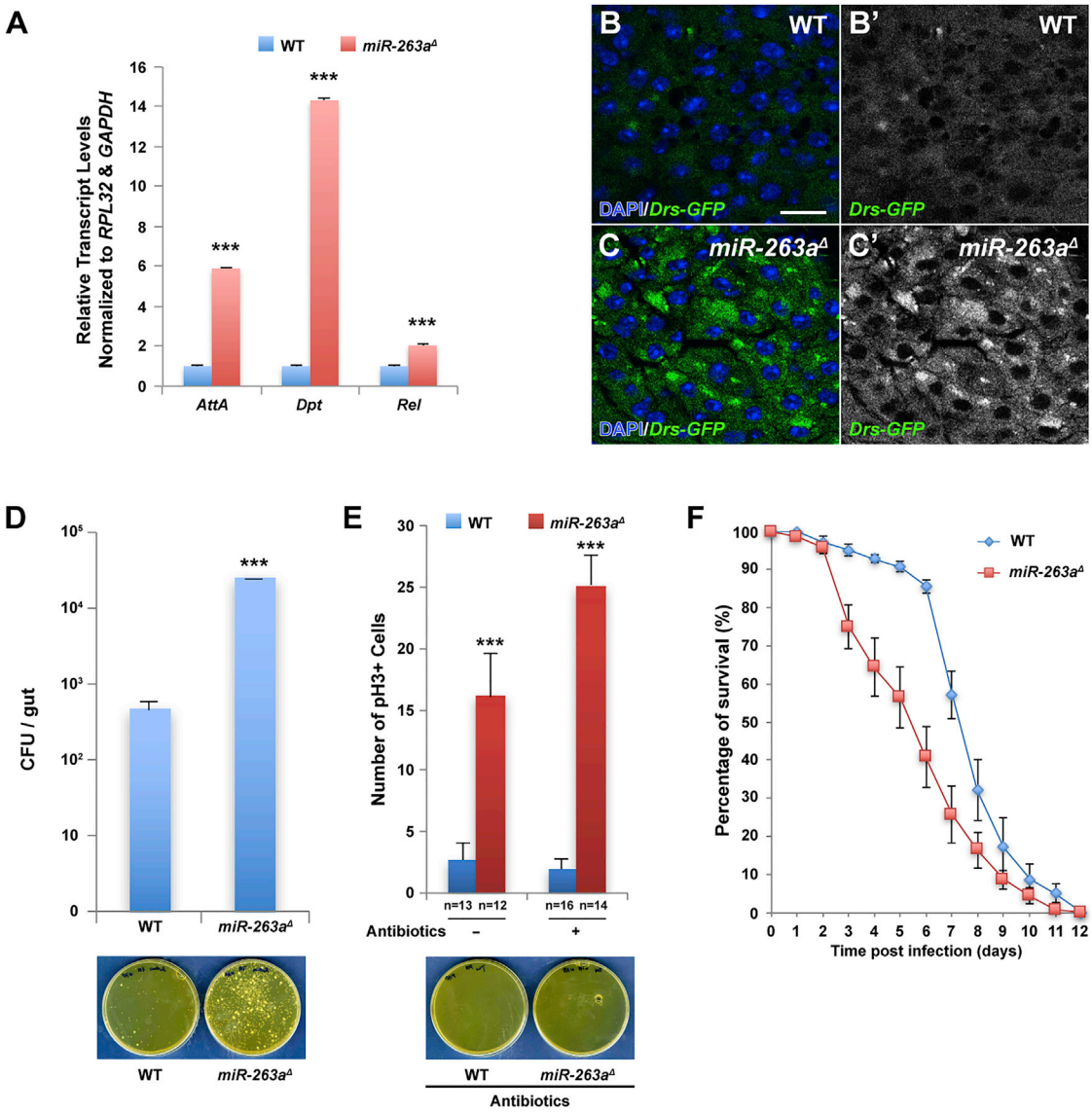

Figure 6. Increased Activation of the Imd Pathway and Susceptibility to Bacterial Infection in *miR-263a* Mutants

(A) Significant increase in the relative transcript levels of the antimicrobial peptides was detected in *miR-263a* mutant midguts by qPCR.

(B–C′) Expression of *Drs-GFP* in the posterior midgut. The expression of *Drs-GFP* is significantly lower in wild-type (WT) (B and B′) than in *miR-263a* mutants (C and C′). The scale bar represents 10 μm.

(D) Internal bacterial load significantly increased in the *miR-263a* mutants. Error bars indicate SEM. Wild-type and *miR-263a* mutant flies homogenates were spread on the plate. The bacteria colonies are shown in the lower panel.

(E) The average number of $pH3^+$ cells in the posterior midguts after antibiotics treatment for 16 days. Feeding antibiotics had no effect on the hyperproliferation of ISCs observed in the *miR-263a* mutant midguts. Lower panel shows the bacteria colonies on medium plate spread with antibiotics fed wild-type and *miR-263a* mutant homogenate. Internal bacteria were absent in both wild-type and *miR-263a* mutant flies fed for 16 days with food containing antibiotics. n denotes the number of posterior midguts examined for each genotype. Error bars indicate SEM.

(F) Survival analysis of wild-type and *miR-263a* mutant flies upon oral infection with *P. aeruginosa*. The *miR-263a* mutant flies exhibited significant increase in lethality 3 days after infection. Error bars indicate SEM.

***$p < 0.001$ (two-tailed t test). See also Figure S6.

Next, we investigated whether *miR-263a* mutants are more susceptible to bacterial infection using *Pseudomonas aeruginosa*, a major pathogen in the CF lung (Ohman and Chakrabarty, 1982; Palmer et al., 2005). Oral infection with *P. aeruginosa* in wild-type flies causes both acute and chronic infection to which the flies ultimately succumb (Mulcahy et al., 2011). After 72 hr of oral infection, *miR-263a* mutants exhibited a higher susceptibility than wild-type (Figure 6F), indicating that structurally compromised PM leads to increased bacterial infection. Together, our results show that structurally compromised PM in the *miR-263a* mutants allow for more bacterial infection and have elevated levels of the antimicrobial peptides due to

activation of the Imd pathway. This increased susceptibility to bacterial infection is likely an indirect result from structurally compromised PM, and is not the cause of ISC overproliferation.

miR-263a Mutants Disrupt Intestinal pH Homeostasis

In *Drosophila* adults the anterior midgut region is neutral in pH, and is followed by an acidic zone (pH < 4) called the copper-cell region. The posterior midgut is mildly alkaline (pH 7–9) and is followed by the hindgut, which is slightly acidic (pH 5) (Dubreuil, 2004; Shanbhag and Tripathi, 2009) (Figure S6A). To assess how structurally compromising the PM influences intestinal physiology, we tested whether intestinal pH homeostasis was perturbed in the *miR-263a* mutants. The intestinal pH was monitored colorimetrically by feeding animals phenol red as previously described (Shanbhag and Tripathi, 2009). In control midguts only the posterior midgut is dark red, reflecting its high pH (Figure S6A). However, in the *miR-263a* mutant, almost the entire length of the midgut is alkaline, as revealed by expansion of the dark-red zone (Figure S6B). Alkalization of the mutant midgut is suppressed by overexpressing *miR-263a* or by knocking down *Nach* (Figures S6C and S6D). These results indicate that the absence of *miR-263a* and subsequent increase in Nach activity disrupts intestinal pH homeostasis, which may provide a more favorable environment for bacterial survival.

DISCUSSION

In this study, we describe a mechanism by which a miRNA regulates ENaC to maintain ISC and osmotic homeostasis in the *Drosophila* midgut epithelium. Specifically, we identified an evolutionarily conserved miRNA, *miR-263a*, which directly and indirectly regulates the expression of ENaC subunits (Figure 7). Strikingly, the phenotypes of *miR-263a* mutants are reminiscent of the pathophysiology of CF.

In CF, two different models have been proposed regarding the role of hydration and salt concentration in normal airway defense (Guggino, 2001). The hydration model proposes that increased absorption of fluid by the epithelium leads to dehydrated mucus and impaired mucociliary clearance that contributes to the establishment of an environment promoting colonization of the lungs by bacteria. In contrast, the salt model proposes that the salt content of airway fluid in CF is too high and thus prevents salt-sensitive defensin molecules in the airway surface liquid from killing bacteria, leading to increased susceptibility to lung infections. In *Drosophila*, the phenotypes associated with perturbation of ENaC are consistent with the hydration model, as misregulation of ENaC subunits in *miR-263a* mutants result in increased sodium reabsorption across the midgut epithelium. Furthermore, we observed a dehydration-like phenotype of the PM, which is analogous to mucous secretions in the vertebrate digestive tract. Consistent with the PM providing protection against abrasive food particles and pathogens, *miR-263a* mutants appear more susceptible to bacterial infections as they succumb to *P. aeruginosa* infection more rapidly than the controls. In addition, we observed increased bacterial load and antimicrobial peptide levels, and disruption of the intestinal pH in *miR-263a* mutants. Interestingly, ECs in *miR-263a* mutants appear swollen, which is likely due to increased water reabsorption through osmosis. Finally, we observed an activation of stressed pathways characteristic of damaged ECs, which correlates with increased proliferation of ISCs.

Consistent with previous reports that cell swelling can activate the JNK pathway (Berl et al., 1997; Huangfu et al., 2006; Sinning et al., 1997), JNK signaling is activated in *miR-263a* mutants that have large ECs. In addition, the JAK/STAT and EGFR pathways that regulate ISC proliferation (Biteau and Jasper, 2011; Buchon et al., 2010; Jiang and Edgar, 2011; Jiang et al., 2009; Osman et al., 2012; Zhou et al., 2013) are hyperactivated. Similarly, in CF airway and small intestine epithelia, cells in the airway epithelium and submucosal glands are more proliferative than cells in non-CF airways (Leigh et al., 1995). In addition, in all CF mouse models in which CFTR has been deleted, goblet cell hyperplasia was observed in the small intestine (Gallagher and Gottlieb, 2001).

Although the existence of *Drosophila* CFTR is yet to be determined, given its phenotypic similarities to the pathophysiology of CF, *miR-263a* mutants may provide a cost-effective and high-throughput animal model for identifying potential therapeutics that can specifically target ENaC in vivo, as the *Drosophila* gut is amenable to large-scale small-molecule screens (Markstein et al., 2014). In addition, *miR-183* might itself be a potential therapeutic agent for regulating ENaC activity in CF, based on our data that overexpression of *miR-183* can directly target the expression of all three ENaC subunits in CFBE41o$^-$ cells (Figure S7). Thus, possibly a combinational therapy for CF using the CFTR potentiator, Ivacaftor (also known as Kalydeco [McPhail and Clancy, 2013]), which improves the transport of chloride through the mutated CFTR, together with overexpression of *miR-183*, could be imagined.

EXPERIMENTAL PROCEDURES

Drosophila Stocks and Genetics

The following *Drosophila* stocks were used in this study: *miR-263a*$^{\Delta}$, *miR-263a*$^{\Delta}$*-Gal4*, and *miR-263b*$^{\Delta}$ (Hilgers et al., 2010); *bft*^{24} (Hardiman et al., 2002); *UAS-miR-263a* (Bejarano et al., 2012); *puc-LacZ* (*puc*^{E69}) (Martin-Blanco et al., 1998); *10XSTAT-GFP* (Bach et al., 2007); *Drs-GFP*; *esg-LacZ* (*esg*^{k00606}); *Dl-LacZ* (*Dl*^{05151}) (Bloomington Stock 11651); *Myo1A-Gal4* (Jiang et al., 2009); *hsFlp*, *Tub-Gal4*, *UAS-GFP/FM7*; *Tub-Gal80*, *FRT40A/CyO* (Karpowicz et al., 2010); *Nach RNAi* (JF02566) (Bloomington Stock 27262); *Nach RNAi* (VDRC45921) (Vienna Drosophila Resource Center Stock 45921); *ppk6 RNAi* (JF01919) (Bloomington Stock 25880); *ppk16 RNAi* (JF01931) (Bloomington Stock 25890); and *ppk28 RNAi* (JF02153) (Bloomington Stock 31878). An FRT site (FRT40A) was introduced by recombination onto the chromosome arm carrying the *miR-263a*$^{\Delta}$. All stocks were maintained and crossed at 25°C. For MARCM clones, 2- to 3-day-old adult flies were heat shocked for 1 hr at 37°C to induce clones and kept at 25°C for 14–21 days until dissection. The genotypes used were: (1) *hsFlp*, *Tub-Gal4*, *UAS-GFP/FM7*; *Tub-Gal80*, *FRT40A/CyO*; *Dl-LacZ*; (2) *hsFlp*, *Tub-Gal4*, *UAS-GFP/FM7*; *Tub-Gal80*, *FRT40A*, *miR-263a*$^{\Delta}$*/CyO*; *Dl-LacZ*; (3) *hsFlp*, *Tub-Gal4*, *UAS-GFP/FM7*; *Tub-Gal80*, *FRT40A/CyO*; *puc-LacZ*; and (4) *hsFlp*, *Tub-Gal4*, *UAS-GFP/FM7*; *Tub-Gal80*, *FRT40A*, *miR-263a*$^{\Delta}$*/CyO*; *puc-LacZ*.

Generation of *UAS-Nach* Transgenic Fly

For construction of *UAS-Nach* plasmid, *Nach* genomic fragment was amplified using specific primers (F, 5′-CGGAATTCATGGGCCACAGGAGGAGC TGAAGC-3′; R, 5′-GCTCTAGATTACGATTTGTGAATTATGAAAACTGAT-3′). The amplified fragment was digested with *Eco*RI and *Xba*I, and was ligated into the linearized *pWALIUM10-moe* vector. The transgenic fly was established by injecting *UAS-Nach* plasmid into flies carrying attP docking site, attP2, located on the third chromosome.

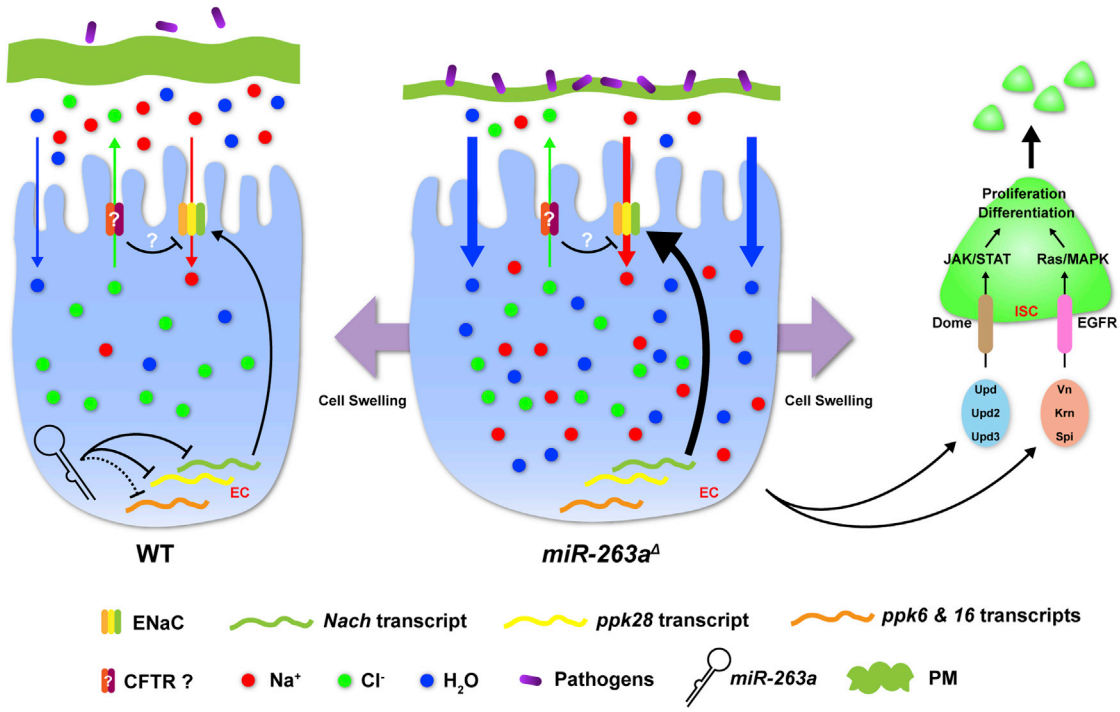

Figure 7. Model of Regulation of ENaC by *miR-263a*

miR-263a maintains ISC and osmotic homeostasis in the midgut epithelium by directly and indirectly regulating the expression of ENaC subunits. See also Figure S7.

Immunostaining of the Midgut

Prior to dissection, flies were fed on 5% sucrose for ~3 hr to remove food from the midgut. Female guts were dissected in 1× PBS and fixed in 4% paraformaldehyde diluted with 1× PBS for 30 min. Samples were washed with 1× PBS, and blocked for 30 min in 1× PBS, 5% donkey serum, and 0.1% Triton X-100. Samples were incubated overnight at 4°C using the following antibodies: mouse anti-Armadillo (1:50), mouse anti-Delta (1:50), mouse anti-Prospero (1:100) (Developmental Studies Hybridoma Bank), rabbit anti-β-galactosidase (1:1,000; Cappel), mouse anti-β-galactosidase (1:1,000; Promega), rabbit anti-phospho-histone H3 (1:10,000; Millipore), and rabbit anti-P-p44/42 MAPK (dpERK) (1:200; Cell Signaling). Primary antibodies were detected using anti-mouse or anti-rabbit secondary antibodies conjugated to Alexa Fluor 488 and 594 (1:1,000; Invitrogen). Alexa Fluor 488-conjugated phalloidin (1:100; Molecular Probes) was used to stain F-actin. Fluorescent images were acquired with a Leica TCS SP2 AOBS.

Quantification of EC Size

miR-263a mutant clones were generated using the MARCM approach as described above and immunostained using anti-Armadillo to label all cell membranes. The surface area of the *miR-263a* mutant ECs (GFP^+) and their respective nuclei were measured using ImageJ (NIH). The surface area of the wild-type ECs (GFP^-), right next to the mutant ECs (GFP^+), was used as control. For analysis of the cell volume, serial sections (~19–32 sections per individual EC) of individual ECs in the MARCM clones were taken using confocal microscopy. Total cell volume was calculated as follows:

$$\text{Cell volume } (\mu m^3) = \text{Total cell surface area } (\mu m^2) \times \text{Thickness } (\mu m)/\text{Sections} \times \text{Number of sections}$$

miR-183 Overexpression in CFBE41o⁻ Cells

Immortalized CFBE41o⁻ cells were obtained from Dr. D. Gruenert (California Pacific Medical Center Research Institute). CFBE41o⁻ cells were grown in MEM (minimum essential medium with Earle's salt; Life Technologies) supplemented with 10% fetal bovine serum (Life Technologies), 2 mM L-glutamine (Life Technologies), and 1% penicillin/streptomycin (Life Technologies) in 75-cm^2 flasks and maintained in a 37°C humidified incubator containing 5% CO_2. Cells were routinely grown on flasks coated with an extracellular matrix containing fibronectin/vitrogen/BSA. The *miR-183* overexpression experiment was performed on 6-well plates. The day before transfection, each well was seeded with 300,000 cells. Next day, either 1.0 μg of *pcDNA3.1-miR-183* or empty *pcDNA3.1* (control) plasmid was transfected using Effectene Transfection Reagent (Qiagen). After 72 hr, total RNA was extracted using TRIzol Reagent (Invitrogen). The *pcDNA3.1-miR-183* plasmid was constructed by amplifying a 399-nt fragment from HEK293 genomic DNA using specific primers (F, 5′-CTAGCTAGCAAGGTCATCTTGGGCTGATG-3′; R, 5′-CCGCTCGAGT CTCTGGGGACACACTGGAC-3′). The amplified fragment was digested with *Nhe*I and *Xho*I, and was ligated into the linearized *pcDNA3.1* vector.

Nach Antibody

Nach antibody was generated in rabbit against a peptide containing amino acids 516–535 (CPKANDTHSKEQKSVFIIHKS) and affinity-purified at YenZym Antibodies.

Western Blots

Lysates prepared from dissected adult female midguts were separated by SDS-PAGE, blotted onto nitrocellulose membrane, and subjected to western analysis using antibodies against Nach (1:500) and α-tubulin (1:1,000; Sigma). Blots were subsequently incubated with horseradish peroxidase-conjugated goat secondary antibody (Amersham), and processed for chemiluminescence (Pierce). For quantification of band intensity, the raw images were analyzed using ImageJ (NIH).

Sodium Green Assay

Adult female flies, 14–16 days old, were fed 2 μM cell-permeant Sodium Green Tetraacetate Indicator (Invitrogen) diluted in 5% sucrose for 3–4 hr, and dissected and fixed in 4% paraformaldehyde diluted with 1× PBS for 30 min. After a brief wash with 1× PBS, samples were mounted, and images were taken immediately using a Leica TCS SP2 AOBS. For quantification of Sodium Green fluorescence, the raw images were analyzed using ImageJ (NIH).

Electron Microscopy

Dissected midguts were fixed overnight in 0.1 M sodium cacodylate buffer (pH 7.4) containing 2.5% glutaraldehyde and 2% paraformaldehyde. The fixed samples were washed three times in distilled water, fixed again with 1% osmium tetroxide and 1.5% potassium ferrocyanide for 1 hr, and washed three times in distilled water. The samples were then washed in 1% maleate buffer and incubated in 1% aqueous uranyl acetate in 1% maleate buffer for 1 hr, followed by two washes in 1% maleate buffer and subsequent dehydration in grades of alcohol. The samples were put in propylene oxide for 1 hr and embedded with a solution of 50% propylene oxide and 50% TAAB Epon overnight. Next day, samples were embedded in fresh TAAB Epon and polymerized for 2 days at 60°C. Ultrathin sections (~60 nm) were cut on a Reichert Ultracut-S microtome, picked up onto copper grids, and stained with lead citrate. The sections were examined in a JEOL 1200EX transmission electron microscope, and images were recorded with an AMT 2k CCD camera.

Internal Bacterial Load

Age-matched cohorts of ten control and ten *miR-263a* mutant flies were co-housed in the same vial and were transferred to a new vial every other day. Three vials were used for the analysis. For culture of the internal commensal bacteria, four flies were washed with 70% ethanol for 2 min and rinsed with sterile water twice to remove the external bacteria. Four flies were homogenized in 400 μL of MRS medium and serial dilutions were plated on the MRS plates. Plates were incubated at 30°C for 48–72 hr before counting CFUs.

Bacterial Infection Assays

P. aeruginosa PA14 was grown on Luria-Bertani (LB) medium overnight. The following morning, 200 μL of overnight culture was added to 10 mL of LB medium and cultured for another 6–8 hr to reach OD_{600} 1.5. Bacteria/sucrose feeding solution was prepared by mixing 1 mL of the bacteria solution with 4 mL of sucrose solution to reach 4% sucrose final concentration. Bacterial infection assay was performed by placing 20 1- to 3-day-old female flies into individual vials containing Kimwipes containing bacteria/sucrose feeding solution at 25°C. Seven vials of each genotype were used. The number of dead flies was recorded every 24 hr. Flies were transferred to new vials with freshly prepared bacteria/sucrose solution after 3 days.

Feeding Assays

DSS and bleomycin feeding assays were performed as previously described (Ren et al., 2010). In brief, 11- to 13-day-old female flies were fed either 5% DSS or 25 μg/mL of bleomycin (Sigma) dissolved in 5% sucrose solution for 3 days at 25°C. For antibiotics feeding assays, standard laboratory fly food containing 30 μg/mL kanamycin, 100 μg/mL ampicillin, and 34 μg/mL chloramphenicol was fed to newly eclosed female flies. Flies were transferred to food with fresh antibiotics every 1–2 days. After 16 days, midguts were dissected and examined.

Gut pH Assay

The gut pH was assessed by feeding 14- to 16-day-old female flies 0.2% phenol red dissolved in 5% sucrose solution for 3 hr at 25°C. The colors of the guts were photographed immediately after dissection with Zeiss Axioskop 2 compound microscope.

SUPPLEMENTAL INFORMATION

Supplemental Information includes Supplemental Experimental Procedures, seven figures, and one table and can be found with this article online at http://dx.doi.org/10.1016/j.devcel.2016.11.023.

AUTHOR CONTRIBUTIONS

K.K. and R.-J.H. conceived, designed, and performed the experiments; K.K., R.-J.H., and N.P. analyzed the data and wrote the paper.

ACKNOWLEDGMENTS

We thank Drs. S. Cohen, P. Watnick, and Rolf Bodmer for flies. We thank Dr. D. Gruenert for providing the CFBE41o$^-$ cells. We thank the Transgenic RNAi Resource Project, Vienna Drosophila Resource Center, and the Bloomington Drosophila Stock Center for flies, the Developmental Studies Hybridoma Bank for monoclonal antibodies, and the Drosophila RNAi Screening Center (Harvard Medical School) for plate-reader equipment. We thank D. Doupé for sharing unpublished results. We also thank M.-L. Samson, L. Rabinow, S. Mohr, R. Viswanatha, L. Perkins, R. Boucher, and members of the Perrimon laboratory for discussion and critical comments on the manuscript. This work was supported in part by the STARR Foundation (I8-A8-030) and by the NIH (grant R01 GM084947) (N.P.). R.-J.H. is supported by the Jane Coffin Childs Foundation. N.P. is a Howard Hughes Medical Institute investigator.

Received: July 19, 2016
Revised: November 4, 2016
Accepted: November 26, 2016
Published: December 22, 2016

REFERENCES

Amorino, G.P., and Fox, M.H. (1995). Intracellular Na^+ measurements using sodium green tetraacetate with flow cytometry. Cytometry *21*, 248–256.

Bach, E.A., Ekas, L.A., Ayala-Camargo, A., Flaherty, M.S., Lee, H., Perrimon, N., and Baeg, G.H. (2007). GFP reporters detect the activation of the *Drosophila* JAK/STAT pathway in vivo. Gene Expr. Patterns *7*, 323–331.

Bejarano, F., Bortolamiol-Becet, D., Dai, Q., Sun, K., Saj, A., Chou, Y.T., Raleigh, D.R., Kim, K., Ni, J.Q., Duan, H., et al. (2012). A genome-wide transgenic resource for conditional expression of *Drosophila* microRNAs. Development *139*, 2821–2831.

Berdiev, B.K., Qadri, Y.J., and Benos, D.J. (2009). Assessment of the CFTR and ENaC association. Mol. Biosyst. *5*, 123–127.

Berl, T., Siriwardana, G., Ao, L., Butterfield, L.M., and Heasley, L.E. (1997). Multiple mitogen-activated protein kinases are regulated by hyperosmolality in mouse IMCD cells. Am. J. Physiol. *272*, F305–F311.

Bhalla, V., and Hallows, K.R. (2008). Mechanisms of ENaC regulation and clinical implications. J. Am. Soc. Nephrol. *19*, 1845–1854.

Bianchi, L., and Driscoll, M. (2002). Protons at the gate: DEG/ENaC ion channels help us feel and remember. Neuron *34*, 337–340.

Biteau, B., and Jasper, H. (2011). EGF signaling regulates the proliferation of intestinal stem cells in *Drosophila*. Development *138*, 1045–1055.

Boucher, R.C. (2007). Cystic fibrosis: a disease of vulnerability to airway surface dehydration. Trends Mol. Med. *13*, 231–240.

Brennecke, J., Stark, A., Russell, R.B., and Cohen, S.M. (2005). Principles of microRNA-target recognition. PLoS Biol. *3*, e85.

Buchon, N., Broderick, N.A., Kuraishi, T., and Lemaitre, B. (2010). *Drosophila* EGFR pathway coordinates stem cell proliferation and gut remodeling following infection. BMC Biol. *8*, 152.

Canessa, C.M., Schild, L., Buell, G., Thorens, B., Gautschi, I., Horisberger, J.D., and Rossier, B.C. (1994). Amiloride-sensitive epithelial Na^+ channel is made of three homologous subunits. Nature *367*, 463–467.

Chalfie, M., and Sulston, J. (1981). Developmental genetics of the mechanosensory neurons of *Caenorhabditis elegans*. Dev. Biol. *82*, 358–370.

Chalfie, M., and Wolinsky, E. (1990). The identification and suppression of inherited neurodegeneration in *Caenorhabditis elegans*. Nature *345*, 410–416.

Chen, E.Y., Yang, N., Quinton, P.M., and Chin, W.C. (2010). A new role for bicarbonate in mucus formation. Am. J. Physiol. Lung Cell Mol. Physiol. *299*, L542–L549.

Davies, J.R., Svitacheva, N., Lannefors, L., Kornfalt, R., and Carlstedt, I. (1999). Identification of MUC5B, MUC5AC and small amounts of MUC2 mucins in cystic fibrosis airway secretions. Biochem. J. *344*, 321–330.

Driscoll, M., and Chalfie, M. (1991). The mec-4 gene is a member of a family of *Caenorhabditis elegans* genes that can mutate to induce neuronal degeneration. Nature *349*, 588–593.

Dubreuil, R.R. (2004). Copper cells and stomach acid secretion in the *Drosophila* midgut. Int. J. Biochem. Cell Biol. *36*, 745–752.

Gabay, L., Seger, R., and Shilo, B.Z. (1997). MAP kinase in situ activation atlas during *Drosophila* embryogenesis. Development *124*, 3535–3541.

Gallagher, A.M., and Gottlieb, R.A. (2001). Proliferation, not apoptosis, alters epithelial cell migration in small intestine of CFTR null mice. Am. J. Physiol. Gastrointest. Liver Physiol. *281*, G681–G687.

Gangaraju, V.K., and Lin, H. (2009). MicroRNAs: key regulators of stem cells. Nat. Rev. Mol. Cell Biol. *10*, 116–125.

Garty, H., and Palmer, L.G. (1997). Epithelial sodium channels: function, structure, and regulation. Physiol. Rev. *77*, 359–396.

Grubb, B.R., and Gabriel, S.E. (1997). Intestinal physiology and pathology in gene-targeted mouse models of cystic fibrosis. Am. J. Physiol. *273*, G258–G266.

Guggino, W.B. (2001). Cystic fibrosis salt/fluid controversy: in the thick of it. Nat. Med. *7*, 888–889.

Hardiman, K.E., Brewster, R., Khan, S.M., Deo, M., and Bodmer, R. (2002). The bereft gene, a potential target of the neural selector gene cut, contributes to bristle morphogenesis. Genetics *161*, 231–247.

Hauber, H.P., Tsicopoulos, A., Wallaert, B., Griffin, S., McElvaney, N.G., Daigneault, P., Mueller, Z., Olivenstein, R., Holroyd, K.J., Levitt, R.C., et al. (2004). Expression of HCLCA1 in cystic fibrosis lungs is associated with mucus overproduction. Eur. Respir. J. *23*, 846–850.

Henderson, A.G., Ehre, C., Button, B., Abdullah, L.H., Cai, L.H., Leigh, M.W., DeMaria, G.C., Matsui, H., Donaldson, S.H., Davis, C.W., et al. (2014). Cystic fibrosis airway secretions exhibit mucin hyperconcentration and increased osmotic pressure. J. Clin. Invest. *124*, 3047–3060.

Hilgers, V., Bushati, N., and Cohen, S.M. (2010). *Drosophila* microRNAs 263a/b confer robustness during development by protecting nascent sense organs from apoptosis. PLoS Biol. *8*, e1000396.

Hovenberg, H.W., Davies, J.R., and Carlstedt, I. (1996). Different mucins are produced by the surface epithelium and the submucosa in human trachea: identification of MUC5AC as a major mucin from the goblet cells. Biochem. J. *318*, 319–324.

Hu, Y., Flockhart, I., Vinayagam, A., Bergwitz, C., Berger, B., Perrimon, N., and Mohr, S.E. (2011). An integrative approach to ortholog prediction for disease-focused and other functional studies. BMC Bioinformatics *12*, 357.

Huang, M., and Chalfie, M. (1994). Gene interactions affecting mechanosensory transduction in *Caenorhabditis elegans*. Nature *367*, 467–470.

Huangfu, W.C., Omori, E., Akira, S., Matsumoto, K., and Ninomiya-Tsuji, J. (2006). Osmotic stress activates the TAK1-JNK pathway while blocking TAK1-mediated NF-kappaB activation: TAO2 regulates TAK1 pathways. J. Biol. Chem. *281*, 28802–28810.

Jiang, H., and Edgar, B.A. (2011). Intestinal stem cells in the adult *Drosophila* midgut. Exp. Cell Res. *317*, 2780–2788.

Jiang, H., Patel, P.H., Kohlmaier, A., Grenley, M.O., McEwen, D.G., and Edgar, B.A. (2009). Cytokine/Jak/Stat signaling mediates regeneration and homeostasis in the *Drosophila* midgut. Cell *137*, 1343–1355.

Karpowicz, P., Perez, J., and Perrimon, N. (2010). The Hippo tumor suppressor pathway regulates intestinal stem cell regeneration. Development *137*, 4135–4145.

Kuraishi, T., Binggeli, O., Opota, O., Buchon, N., and Lemaitre, B. (2011). Genetic evidence for a protective role of the peritrophic matrix against intestinal bacterial infection in *Drosophila* melanogaster. Proc. Natl. Acad. Sci. USA *108*, 15966–15971.

Lee, T., and Luo, L. (2001). Mosaic analysis with a repressible cell marker (MARCM) for *Drosophila* neural development. Trends Neurosci. *24*, 251–254.

Leigh, M.W., Kylander, J.E., Yankaskas, J.R., and Boucher, R.C. (1995). Cell proliferation in bronchial epithelium and submucosal glands of cystic fibrosis patients. Am. J. Respir. Cell Mol. Biol. *12*, 605–612.

Liehl, P., Blight, M., Vodovar, N., Boccard, F., and Lemaitre, B. (2006). Prevalence of local immune response against oral infection in a *Drosophila*/*Pseudomonas* infection model. PLoS Pathog. *2*, e56.

Lingueglia, E., Voilley, N., Waldmann, R., Lazdunski, M., and Barbry, P. (1993). Expression cloning of an epithelial amiloride-sensitive Na^+ channel. A new channel type with homologies to *Caenorhabditis elegans* degenerins. FEBS Lett. *318*, 95–99.

Mall, M., Grubb, B.R., Harkema, J.R., O'Neal, W.K., and Boucher, R.C. (2004). Increased airway epithelial Na^+ absorption produces cystic fibrosis-like lung disease in mice. Nat. Med. *10*, 487–493.

Markstein, M., Dettorre, S., Cho, J., Neumuller, R.A., Craig-Muller, S., and Perrimon, N. (2014). Systematic screen of chemotherapeutics in *Drosophila* stem cell tumors. Proc. Natl. Acad. Sci. USA *111*, 4530–4535.

Martin-Blanco, E., Gampel, A., Ring, J., Virdee, K., Kirov, N., Tolkovsky, A.M., and Martinez-Arias, A. (1998). Puckered encodes a phosphatase that mediates a feedback loop regulating JNK activity during dorsal closure in *Drosophila*. Genes Dev. *12*, 557–570.

Mathieu, J., and Ruohola-Baker, H. (2013). Regulation of stem cell populations by microRNAs. Adv. Exp. Med. Biol. *786*, 329–351.

Matsui, H., Grubb, B.R., Tarran, R., Randell, S.H., Gatzy, J.T., Davis, C.W., and Boucher, R.C. (1998). Evidence for periciliary liquid layer depletion, not abnormal ion composition, in the pathogenesis of cystic fibrosis airways disease. Cell *95*, 1005–1015.

McPhail, G.L., and Clancy, J.P. (2013). Ivacaftor: the first therapy acting on the primary cause of cystic fibrosis. Drugs Today (Barc) *49*, 253–260.

Minta, A., and Tsien, R.Y. (1989). Fluorescent indicators for cytosolic sodium. J. Biol. Chem. *264*, 19449–19457.

Mulcahy, H., Sibley, C.D., Surette, M.G., and Lewenza, S. (2011). *Drosophila* melanogaster as an animal model for the study of *Pseudomonas aeruginosa* biofilm infections in vivo. PLoS Pathog. *7*, e1002299.

Nehme, N.T., Liegeois, S., Kele, B., Giammarinaro, P., Pradel, E., Hoffmann, J.A., Ewbank, J.J., and Ferrandon, D. (2007). A model of bacterial intestinal infections in *Drosophila melanogaster*. PLoS Pathog. *3*, e173.

Ohlstein, B., and Spradling, A. (2007). Multipotent *Drosophila* intestinal stem cells specify daughter cell fates by differential notch signaling. Science *315*, 988–992.

Ohman, D.E., and Chakrabarty, A.M. (1982). Utilization of human respiratory secretions by mucoid *Pseudomonas aeruginosa* of cystic fibrosis origin. Infect Immun. *37*, 662–669.

Okumura, T., Takeda, K., Taniguchi, K., and Adachi-Yamada, T. (2014). Betanu integrin inhibits chronic and high level activation of JNK to repress senescence phenotypes in *Drosophila* adult midgut. PLoS One *9*, e89387.

Osman, D., Buchon, N., Chakrabarti, S., Huang, Y.T., Su, W.C., Poidevin, M., Tsai, Y.C., and Lemaitre, B. (2012). Autocrine and paracrine unpaired signaling regulate intestinal stem cell maintenance and division. J. Cell Sci. *125*, 5944–5949.

Palmer, K.L., Mashburn, L.M., Singh, P.K., and Whiteley, M. (2005). Cystic fibrosis sputum supports growth and cues key aspects of *Pseudomonas aeruginosa* physiology. J. Bacteriol. *187*, 5267–5277.

Patel, P.H., Dutta, D., and Edgar, B.A. (2015). Niche appropriation by *Drosophila* intestinal stem cell tumours. Nat. Cell Biol. *17*, 1182–1192.

Ren, F., Wang, B., Yue, T., Yun, E.Y., Ip, Y.T., and Jiang, J. (2010). Hippo signaling regulates *Drosophila* intestine stem cell proliferation through multiple pathways. Proc. Natl. Acad. Sci. USA *107*, 21064–21069.

Riordan, J.R. (2008). CFTR function and prospects for therapy. Annu. Rev. Biochem. *77*, 701–726.

Ruby, J.G., Stark, A., Johnston, W.K., Kellis, M., Bartel, D.P., and Lai, E.C. (2007). Evolution, biogenesis, expression, and target predictions of a substantially expanded set of *Drosophila* microRNAs. Genome Res. *17*, 1850–1864.

Ryu, J.H., Ha, E.M., Oh, C.T., Seol, J.H., Brey, P.T., Jin, I., Lee, D.G., Kim, J., Lee, D., and Lee, W.J. (2006). An essential complementary role of NF-kappaB pathway to microbicidal oxidants in *Drosophila* gut immunity. EMBO J. *25*, 3693–3701.

Shanbhag, S., and Tripathi, S. (2009). Epithelial ultrastructure and cellular mechanisms of acid and base transport in the *Drosophila* midgut. J. Exp. Biol. *212*, 1731–1744.

Sinning, R., Schliess, F., Kubitz, R., and Haussinger, D. (1997). Osmosignalling in C6 glioma cells. FEBS Lett. *400*, 163–167.

Southall, T.D., Gold, K.S., Egger, B., Davidson, C.M., Caygill, E.E., Marshall, O.J., and Brand, A.H. (2013). Cell-type-specific profiling of gene expression

and chromatin binding without cell isolation: assaying RNA Pol II occupancy in neural stem cells. Dev. Cell *26*, 101–112.

Waldmann, R., Champigny, G., Bassilana, F., Voilley, N., and Lazdunski, M. (1995). Molecular cloning and functional expression of a novel amiloride-sensitive Na^+ channel. J. Biol. Chem. *270*, 27411–27414.

Yi, R., and Fuchs, E. (2012). A miR image of stem cells and their lineages. Curr. Top. Dev. Biol. *99*, 175–199.

Zelle, K.M., Lu, B., Pyfrom, S.C., and Ben-Shahar, Y. (2013). The genetic architecture of degenerin/epithelial sodium channels in *Drosophila*. G3 (Bethesda) *3*, 441–450.

Zhou, F., Rasmussen, A., Lee, S., and Agaisse, H. (2013). The UPD3 cytokine couples environmental challenge and intestinal stem cell division through modulation of JAK/STAT signaling in the stem cell microenvironment. Dev. Biol. *373*, 383–393.